I wish to acknowledge the support given to this work by the Australian Atomic Energy Commission (Research Contract No. 82/X/1) and the Australian Institute of Nuclear Science and Engineering. I am also grateful to Joanne Hodge and Suzanne Swanson for their assistance during the course of this investigation.

References

BURSILL, L. A. & GRZINIC, G. (1980). *Acta Cryst.* B**36**, 2902-2913.
BYSTRÖM, A. & BYSTRÖM, A. M. (1950). *Acta Cryst.* **3**, 146-154.
CADÉE, M. C. & VERSCHOOR, G. C. (1978). *Acta Cryst.* B**34**, 3554-3558.
CHEARY, R. W., HUNT, J. V. & CALAIZIS, P. (1981). *J. Aust. Ceram. Soc.* **17**, 11-12.
CHEARY, R. W. & KWIATKOWSKA, J. C. (1984). *J. Nucl. Mater.* **125**, 236-243.
DRYDEN, J. C. & WADSLEY, A. D. (1958). *Trans. Faraday Soc.* **54**, 1574-1580.
GUHA, J. P., KOLAR, D. & VOLAVSEK, B. (1976). *J. Solid State Chem.* **16**, 49-54.
HOWARD, C. J. (1982). *J. Appl. Cryst.* **15**, 615-620.
HOWARD, C. J., BALL, C. J., DAVIS, L. D. & ELCOMBE, M. M. (1983). *Aust. J. Phys.* **35**, 507-518.
KESSON, S. E. (1983). *Rad. Waste Manage.* **4**, 53-72.
KESSON, S. E. & RINGWOOD, A. E. (1984). *Scientific Basis for Nuclear Waste Management.* VI, pp. 507-512. Amsterdam: Elsevier.
KESSON, S. E. & WHITE, T. J. (1986). *Proc. R. Soc. London Ser. A.* In the press.
KLUG, H. P. & ALEXANDER, L. E. (1974). *X-ray Diffraction Procedures*, ch. 8, pp. 566-617. New York: Wiley-Interscience.
MEGAW, H. D. (1973). *Crystal Structures: A Working Approach*, pp. 333-334. London: Saunders.
O'KEEFFE, M. (1977). *Acta Cryst.* A**33**, 924-927.
POST, J. E., VON DREELE, R. B. & BUSECK, P. R. (1982). *Acta Cryst.* B**38**, 1056-1065.
PRING, A. (1983). PhD thesis, Univ. of Cambridge.
RIETVELD, H. M. (1969). *J. Appl. Cryst.* **2**, 65-71.
ROTH, R. (1981). Annual Report. National Measurement Laboratory, Office for Nuclear Technology. NBSIR 81-2241.
SABINE, T. M. & HEWAT, A. W. (1982). *J. Nucl. Mater.* **110**, 173-177.
SCHMACTEL, J. & MULLER-BUSCHBAUM, H. K. (1980). *Z. Naturforsch. Teil B*, **35**, 332-334.
SINCLAIR, W., MCLAUGHLIN, G. M. & RINGWOOD, A. E. (1980). *Acta Cryst.* B**38**, 245-246.
WILES, D. B. & YOUNG, R. A. (1981). *J. Appl. Cryst.* **14**, 149-150.

Acta Cryst. (1986). B**42**, 236-247

Determination of the Structure of Cu_2ZnGeS_4 Polymorphs by Lattice Imaging and Convergent-Beam Electron Diffraction

BY A. F. MOODIE AND H. J. WHITFIELD

Division of Chemical Physics, CSIRO, PO Box 160, *Clayton, Victoria, Australia* 3168

(*Received* 2 *May* 1985; *accepted* 22 *November* 1985)

Abstract

The structures of two polymorphs of Cu_2ZnGeS_4 have been determined by the use of convergent-beam electron diffraction (CBED) and high-resolution lattice imaging with 200 kV electrons. A tetragonal polymorph with space group $I\bar{4}2m$ and axes $a = 5{\cdot}27$, $c = 10{\cdot}54$ Å was found to be isostructural with Cu_2FeSnS_4. The second polymorph has a pseudo-rhombohedral structure related to $12R$ ($|+++-|_3$) ZnS by ordered replacement of three-quarters of the Zn atoms by Cu and Ge. It can be described in terms of a triply primitive cell with orthogonal axes $a = 36{\cdot}6$, $b = 6{\cdot}55$ and $c = 7{\cdot}52$ Å. The S-atom positions of a trial ideal structure were refined by use of CBED and lattice images. Stacking faults and edge and screw dislocations were observed in this structure in high-resolution lattice images.

Introduction

We have shown previously (Moodie & Whitfield, 1983) that the stacking sequence in small volumes of normal tetrahedral structures can be determined, using a 200 kV electron microscope, and we have illustrated the technique with the compound CuAsSe.

For ternary and quaternary chalcogenides such as $1_2 4 6_3$ and $1_2 2 4 6_4$ the degree of ordering of metal ions depends on the thermal history of the sample. Furthermore small deviations in stoichiometry can determine the final structure (*e.g.* Cu_2GeS_3) while different polytypes may be stable at high and low temperatures (*e.g.* $CuSiS_3$).

We have found that convergent-beam electron diffraction combined with high-resolution lattice imaging allows both characterization and structure determination on crystal fragments from a matrix

0108-7681/86/030236-12$01.50

which has not reached equilibrium and contains a variety of structures differing in stacking patterns and degree of cation order, the crystallite size often being too small for study by X-ray diffraction.

In the present paper we show that for the simple binary chalcogenides ZnS and CdS in appropriate orientation and with appropriate defect of focus both periodic and aperiodic stacking can be read directly from the images. We then describe the extension of the techniques to the determination of the structures of two polymorphs of Cu_2ZnGeS_4. One form has the stannite structure and the other has a wurtzite-type superlattice with the unusual stacking sequence *hhcc*. This material is a searching test of the technique as the scattering factors and atomic radii of Cu, Zn and Ge are quite similar. As a consequence the sublattice diffraction peaks are not markedly affected by the degree of ordering of cations in the material, and the superlattice reflections are correspondingly weak.

Experimental and computational

Cu_2ZnGeS_4 was prepared by reacting its constituent elements in stoichiometric proportions in an evacuated silica ampoule followed by annealing for long periods below the melting point to well ordered crystalline material.

Samples were prepared for study in the electron microscope by crushing under alcohol and mounting on holey carbon grids. The JEOL 200 CX electron microscope was used in a configuration (Moodie & Whitfield, 1984) that allowed direct switching between convergent-beam electron diffraction (CBED) and imaging of the same field of view at ultrahigh resolution.

All CBED patterns were taken with a crossover of approximately 500 Å and from specimens which were substantially flat and uniform in thickness with crossover. Thickness and variation in thickness were estimated from detail in upper layer line diffraction discs (for instance, Moodie & Whitfield, 1984). Typically excursions in thickness did not exceed two or three periodicities.

Calculations were carried through using a suite of multislice programs written by D. Lynch. Upper layer line effects were included and unitarity checks run as a routine. The aberration coefficients used in the imaging part of the program were measured optically and convergence in the incident beam measured from the diffraction patterns.

Binary chalcogenides ZnS and CdS

The cubic sphalerite structure viewed along $[1\bar{1}0]$ is shown diagrammatically in Fig. 1. The stacking sequence of slabs is indicated at the left of the diagram in Jagodzinski–Wyckoff notation and of layers at the right of the diagram in *ABC* notation. The classical types of intrinsic and extrinsic stacking faults (Amelinckx, 1979) are shown in Figs. 1(*a*) and 1(*b*) respectively. Both of these have been observed experimentally. In Fig. 2 an intrinsic stacking fault can be immediately located in the lattice image of CdS (cubic $a = 5{\cdot}82$ Å) viewed down $[1\bar{1}0]$ at a defect of focus of −900 Å. This identification has been confirmed by multislice calculations in periodic continuation; and a calculation for a crystal of thickness 200 Å and a defect of focus of −900 Å is shown for comparison. This check is particularly important at such large defects of focus. The rows of holes through the struc-

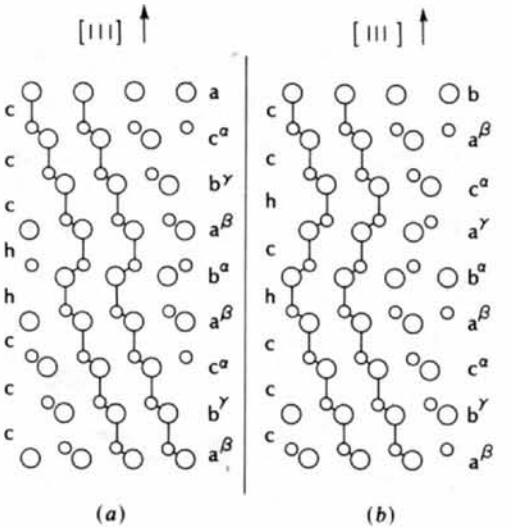

Fig. 1. Projection of the cubic sphalerite structure down $[1\bar{1}0]$ with (*a*) intrinsic and (*b*) extrinsic stacking faults. The stacking sequences of slabs are indicated at the left of the diagrams in Jagodzinski–Wyckoff notation and of layers at the right in *ABC* notation.

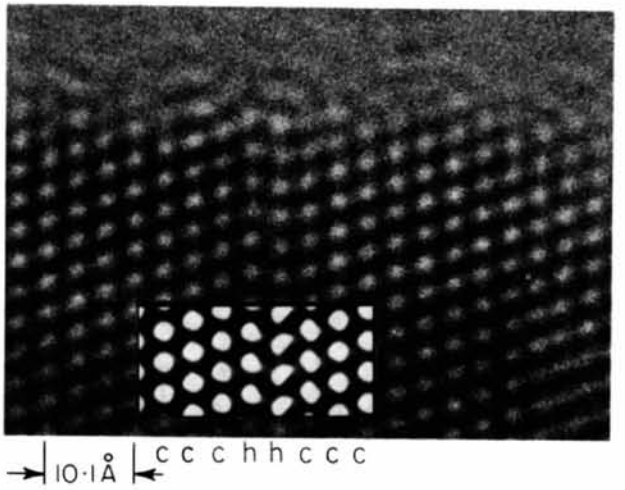

Fig. 2. Lattice image of cubic CdS viewd down $[1\bar{1}0]$, with an intrinsic stacking fault. An image calculated by multislice is shown in the inset.

ture that are the prominent feature of the lattice image are outlined in the diagram of the structure in Fig. 1 to make comparison easy. The appearance of holes through the structure as white in the image is in entire accord with the symmetry arguments previously advanced (Olsen & Spence, 1981).

In Fig. 3 the hexagonal wurtzite structure viewed down [100] is shown diagrammatically with the stacking sequences indicated for the classical single and double stacking faults. In a lattice image of the hexagonal polytype of zinc sulfide (Fig. 4*a*) (a = 3·823, c = 6·257 Å) a double stacking fault is evident as indicated by the stacking sequence and in Fig. 4(*b*) a quadrupole stacking fault is apparent.

At such resolutions the limits for the validity of the charge-density approximation are grossly exceeded in both thickness and defect of focus. It is therefore very surprising to find, as we have, that certain features of the images of such compounds persist through a range of thickness, are almost independent of composition and, at approximately −900 Å defect of focus, map the distribution of holes in a given stacking sequence. Thus with discretion both periodic and aperiodic outline structures can be read off directly.

We believe that this derives from the circumstance that for projections down or very near to specific axes the potential in a wide range of tetrahedrally bonded compounds closely approximates to sharply peaked axially symmetric distributions. Under these conditions Sayre's (1951) relations greatly simplify the dynamical equations, a matter which will be discussed elsewhere.

Quaternary chalcogenide Cu_2ZnGeS_4

The quaternary chalcogenide Cu_2ZnGeS_4 was prepared by reacting its constituent elements in stoichiometric proportions at 1273 K in an evacuated silica ampoule for 6 h, followed by grinding the product to a fine powder and reheating to obtain a homogeneous product.

X-ray powder diffraction patterns of preparations of Cu_2ZnGeS_4 varied with the thermal history of the preparation. Sublattice lines indicated the presence of both wurtzite- and sphalerite-type lattices but superlattice lines were, in general, very weak suggesting that the bulk products consisted of a mixture of polymorphs.

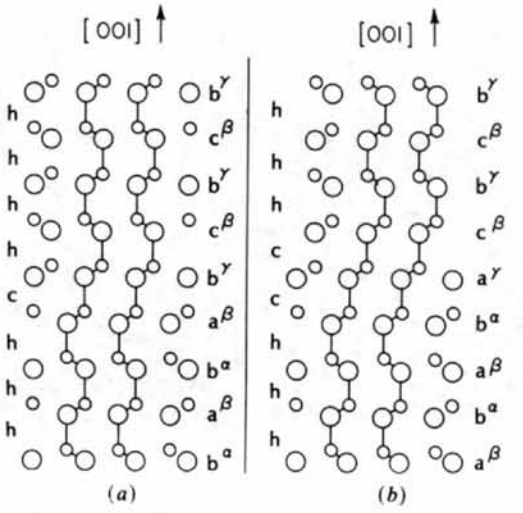

Fig. 3. Projection of the hexagonal wurtzite structure down the [100] direction with (*a*) single and (*b*) double stacking faults.

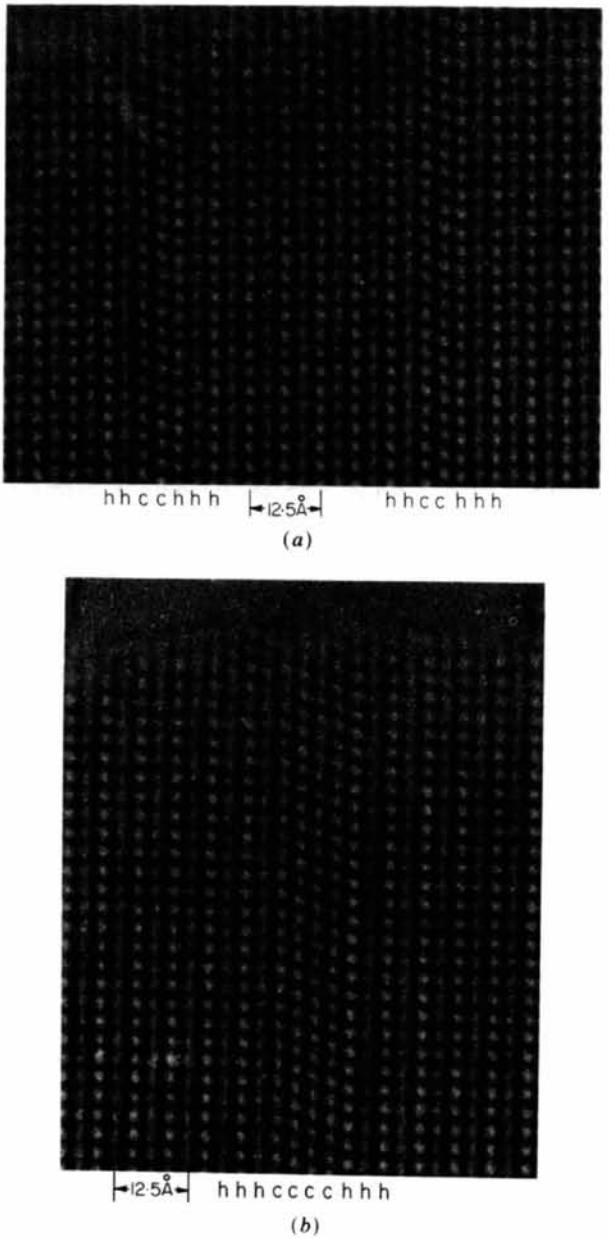

Fig. 4. Lattice images of ZnS viewed (*a*) down [100] with a double stacking fault indicated and (*b*) down [100] with a stacking-fault sequence *hhhccccchhh* indicated.

On grinding selected small crystallites of the material under ethanol and examining with selected-area and convergent-beam electron diffraction and high-resolution imaging, we found that on a micro-scale many crystals were well ordered and as the sample was annealed for longer periods the proportion of well ordered crystals increased. Two principal polymorphs were characterized one being tetragonal and the other pseudo-rhombohedral. The tetragonal polymorph had a cell geometry and CBED pattern that strongly suggested its structure was related to that of sphalerite and indeed the structure was completely elucidated from the CBED patterns.

The second polymorph had CBED patterns for various projections which indicated the unit cell has pseudo-rhombohedral symmetry. For this more complicated structure, the lattice images proved to be of crucial importance in indicating the stacking pattern, and thence the CBED patterns of the various projections were used to unravel the ordering of cations in the superlattice. By visual comparison of the lattice images of the pseudo-rhombohedral Cu_2ZnGeS_4 viewed down its [001] or [$0\bar{2}1$] directions with the lattice image of faulted cubic ZnS (sphalerite) viewed down [$1\bar{1}0$] it was intuitively apparent that the stacking sequence in the quaternary compound is a repeated pattern of the *hhcc* sequence observed in a classical intrinsic stacking fault in sphalerite. Detailed CBED patterns and calculation of intensities of diffraction peaks and multislice calculations of lattice images confirm our intuitive interpretation.

After discussing the details of the structures of the tetrahedral and pseudo-rhombohedral structures (Fig. 5) we present images of crystals that are intergrowths of the two structures.

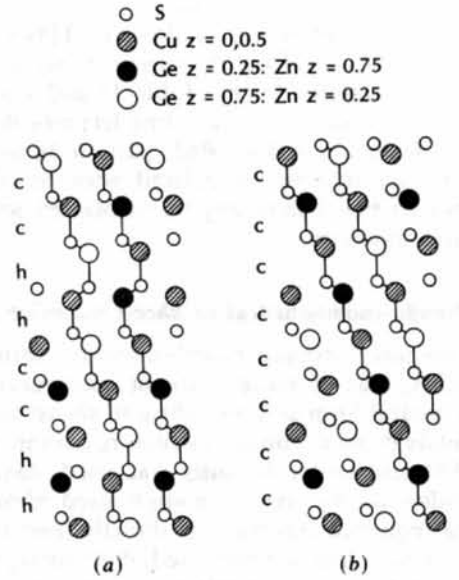

Fig. 5. (*a*) Projection of the pseudo-rhombohedral (*hhcc*) form of Cu_2ZnGeS_4 viewed down [001] with the *hhcc* stacking sequence of slabs indicated. (*b*) Projection of the tetragonal (*ccc*) form of Cu_2ZnGeS_4 down [110] with the stacking sequence indicated.

Tetragonal Cu_2ZnGeS_4

The CBED pattern of a crystal of the tetragonal polymorph of Cu_2ZnGeS_4 viewed down [100] is shown in Fig. 6. The structure is derived from the sphalerite structure by the arrangement of the cations into a well ordered superlattice.

If the metal atoms are ordered in such a way that each S is coordinated to two Cu, one Ge and one Zn atom in accord with the overall stoichiometry of the material, then two possible ordered structures are possible, analogous to those found in Cu_2FeSnS_4 (stannite) and in Na_2ZnSiO_4. The CBED patterns (for instance that of Fig. 6) have such highly characteristic distributions of intensity that the stannite structure was identified with confidence using even the 'ideal' positions. This trial structure which crystallizes (Brockway, 1934) in the noncentrosymmetric tetrahedral space group $I\bar{4}2m$ (No. 121) with S atoms in special positions 8(*i*) $(\frac{1}{2}, \frac{1}{2}, \frac{1}{2})+x, x, z$; $-x, -x, z$; $x, -x, -z$; $-x, x, z$ and all metal atoms in tetrahedral coordination to S in positions 4(*d*) 0, $\frac{1}{2}$, $\frac{1}{4}$; $\frac{1}{2}$, 0, $\frac{1}{4}$; $\frac{1}{2}$, 0, $\frac{3}{4}$; 0, $\frac{1}{2}$, $\frac{3}{4}$ for Cu, 2(*a*) 0, 0, 0; $\frac{1}{2}$, $\frac{1}{2}$, $\frac{1}{2}$ for Zn, 2(*b*) 0, 0, $\frac{1}{2}$; $\frac{1}{2}$, $\frac{1}{2}$, 0 for Ge.

Initially 'ideal' point positions with $x=\frac{1}{4}$, $z=\frac{1}{8}$ were used for the S atoms. These values correspond to equal bond lengths of 2·282 Å for Zn–S, Cu–S and Ge–S. If the S atoms are displaced from these ideal positions to refined positions $x=0{\cdot}256$, $z=0{\cdot}119$ then the bond lengths are 2·32, 2·28 and 2·21 Å for Cu–S, Zn–S and Ge–S respectively in accord with tetrahedral bond radii (Pauling & Huggins, 1934).

In Table 1 are listed the calculated structure factors for 0*kl* and 1*kl* beams for both the 'ideal' and the 'refined' models. Comparison of the two sets of data

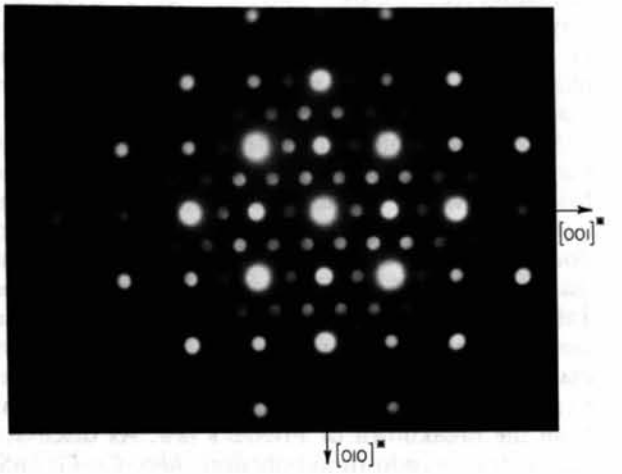

Fig. 6. CBED pattern of tetragonal Cu_2ZnGeS_4 (space group $I\bar{4}2m$, $a=5{\cdot}27$, $c=10{\cdot}54$ Å) viewed down [100].

Table 1. *Calculated 0kl and 1kl structure factors for ideal and refined tetragonal* Cu_2ZnGeS_4

	Ideal		Refined	
h k l	V_R	V_I	V_R	V_I
0 0 2	0·5423	0	0·9711	0
0 0 4	0·6290	0	0·6713	0
0 0 6	0·0772	0	−0·4178	0
0 0 8	3·2461	0	3·1877	0
0 1 1	−0·2792	0	−0·4304	0
0 1 3	−0·1706	0	−0·0743	0
0 1 5	−0·0703	0	0·0108	0
0 1 7	−0·0240	0	−0·0534	0
0 2 0	0·6290	0	0·6396	0
0 2 2	0·1940	0	−0·0546	0
0 2 4	5·5133	0	5·4791	0
0 2 6	0·0363	0	0·3929	0
0 2 8	0·6054	0	0·6540	0
0 3 1	−0·0475	0	0·1311	0
0 3 3	−0·0332	0	−0·1615	0
0 3 5	−0·0180	0	−0·1450	0
0 3 7	−0·0093	0	0·0439	0
0 4 0	3·2461	0	3·2314	0
0 4 2	0·0210	0	0·1115	0
0 4 4	0·6054	0	0·6283	0
0 4 6	0·0127	0	−0·1599	0
0 4 8	1·5643	0	1·5326	0
1 1 0	0·4174	0	0·4244	0
1 1 2	4·8782	−4·2440	4·8787	−4·2259
1 1 4	0·1521	0	0·1479	−0·4443
1 1 6	2·5486	1·8615	2·5480	1·8115
1 1 8	0·0190	0	0·0206	0·3385
1 3 0	0·0628	0	0·0542	0
1 3 2	2·5486	−1·8615	2·5480	−1·8430
1 3 4	0·0310	0	0·0373	0·2213
1 3 6	1·6943	−1·0750	1·6954	−1·401
1 3 8	0·0124	0	0·0094	−0·2187
1 5 0	0·0124	0	0·0176	0
1 5 2	1·2092	−0·7070	1·2095	−0·6920
1 5 4	0·0115	0	0·0072	−0·0910
1 5 6	0·8945	0·5002	0·8937	0·4785
1 5 8	0·0104	0	0·0130	0·1118
1 7 0	−0·0044	0	0·0068	0
1 7 2	0·5211	0·2814	0·5209	0·2706
1 7 4	0·0092	0	0·0116	0·0370
1 7 6	0·4060	−0·2183	0·4065	−0·2052
1 7 8	0·0076	0	0·0060	−0·0507

suggests that the stronger sublattice beam intensities will be less sensitive to small displacements of S atoms from ideal positions than will be the weaker superlattice reflections, particularly those in upper layers. Comparison of intensities of such beams from a many-beam multislice calculation with observed intensities from a CBED pattern would be a sensitive way of refining the structure. This point is discussed in more detail below, where we consider the refinement of the pseudo-rhombohedral *hhcc* Cu_2ZnGeS_4.

As the 0*kl* projection of the tetrahedral form of Cu_2ZnGeS_4 is centrosymmetric the breakdown of Friedel's law will be due entirely to upper layer line interactions. Since the periodicity in the beam direction is only 5·27 Å, this effect is likely to be quite small in both CBED and images. As can be seen from Table 1, although the 0*kl* reflections are all centrosymmetric many of the upper layer 1*kl* beams are markedly noncentrosymmetric suggesting that larger effects may be observed for other projections arising from the breakdown of Friedel's law. As discussed below for pseudo-rhombohedral *hhcc*-Cu_2GeZnS_4 strong effects arising from the noncentrosymmetric nature of the crystal have been observed.

Down the [100] projection of this tetragonal structure there are distinct columns of Cu, Zn, Ge and S atoms. The holes through the structure in this projection, however, are difficult to resolve and the lattice images are not very informative. Examination of models of the structure, however, show that the largest holes through the structure occur in the [021] and [110] projections. Indeed our electron image calculations for various projections confirm that for the [021] and [110] projections imaging conditions exist, on the JEOL 200 kV electron microscope, for which these holes through the structure can be imaged; in these projections faults in the cubic stacking sequence are most readily observed.

In the [021] projection the projected cell is of dimensions $x = 2\sqrt{2}a$, $y = a$ and the repeat distance is $2\sqrt{2}a$. In this projection all metal ions are in columns containing Cu, Zn and Ge in the ratio 2 : 1 : 1.

For the [110] projection the projected cell has dimensions $x = 2a$, $y = \sqrt{2}a$ and the repeat distance along [110] is $\sqrt{2}a$. In this noncentrosymmetric projection there are columns of Cu and columns consisting of equal numbers of Zn and Ge ions.

Fig. 7 is an interesting CBED and Kikuchi pattern obtained for the electron beam incident on the crystal along the [$\bar{8}$21] direction. Patterns of this sort are often particularly effective in disentangling unit-cell relationships in compounds of complicated symmetry. Because the *c* axis of the tetragonal cell is exactly twice the length of the *a* axis, the reciprocal-cell axes [124]*, [01$\bar{2}$]*, and [$\bar{4}$12]* are orthogonal and collinear with the real-space directions [121], [02$\bar{1}$] and [$\bar{8}$21] respectively, that correspond to an alternate orthogonal unit cell of dimensions $a = 15{\cdot}81$, $b = 14{\cdot}906$, $c = 44{\cdot}72$ Å.

The projection of the crystal down [$\bar{8}$21] is noncentrosymmetric as seen from the structure factor for the intense 132 scattered beam (Table 1) and a marked asymmetry is observed between Friedel pairs of reflections for this beam in the CBED pattern. In addition there are asymmetries associated with the diffuse scattering in Fig. 7 that may be associated with the noncentrosymmetry.

Pseudo-rhombohedral or *hhcc*-Cu_2ZnGeS_4

The second pseudo-rhombohedral form of Cu_2ZnGeS_4 was of more frequent occurrence than the tetrahedral form and, as indicated above, in order to elucidate its more complex structure a combination of CBED and lattice imaging was used. Assuming the validity of the approximation used above the stacking sequence was read off directly from images and an outline structure proposed. Preliminary multislice calculations gave satisfactory comparison with observations. Details of the structure were then determined from the CBED patterns. For the outline structure, kinematical structure factors are in the same

orders of magnitude as the observed CBED peaks, a result which is to be anticipated for not too thick crystals if Sayre's relation is obeyed.

The structure is best described in terms of a triply primitive unit cell with orthogonal axes $a = 36{\cdot}6$, $b = 6{\cdot}55$, and $c = 7{\cdot}52$ Å. CBED patterns of this structure are shown in Figs. 8, 9 and 11, selected-area patterns in Figs. 10 and 12, and lattice images in Figs. 13, 14, 15 and 16.

This pseudo-rhombohedral Cu_2ZnGeS_4 has a structure related to that of $12R$ ($|+++-|_3$) ZnS by ordered replacement of three-quarters of the Zn atoms by Cu and Ge atoms. $12R$ ZnS crystallizes in the rhombohedral space group $R3m$, with $Z = 12$ for a hexagonal cell that has axes $a = 3{\cdot}82$ and $c = 37{\cdot}4$ Å.

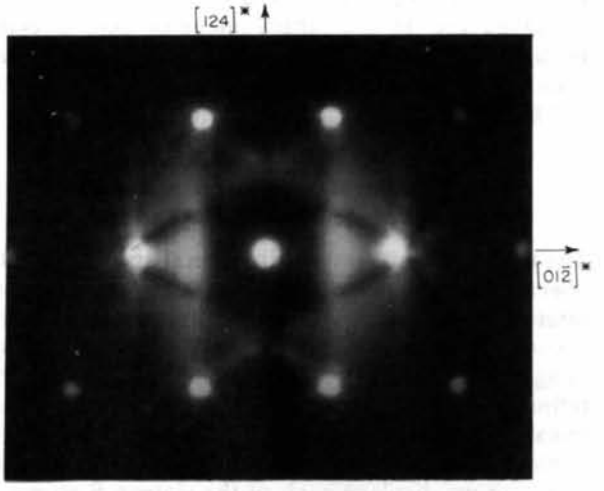

Fig. 7. CBED pattern of the tetragonal form of Cu_2ZnGeS_4 (space group $I\bar{4}2m$, $a = 5{\cdot}27$, $c = 10{\cdot}54$ Å) viewed down [$\bar{8}21$]. Note the noncentrosymmetric Kikuchi pattern.

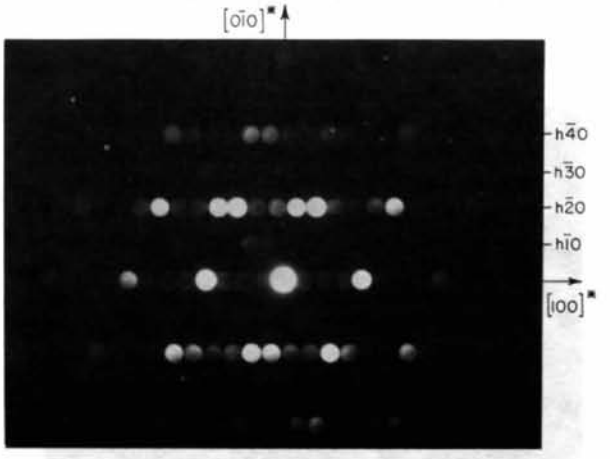

Fig. 8. CBED pattern of the pseudo-rhombohedral (*hhcc*) form of Cu_2ZnGeS_4 ($a = 36{\cdot}6$, $b = 6{\cdot}55$, $c = 7{\cdot}52$ Å) viewed down [001]. The zone axis is close to the centre of the discs as can be seen from the position of the bands and the evident asymmetry arises from the violation of Friedel's law.

All atoms are in the threefold special positions $3(a)$ with coordinates $(0, 0, 0; \frac{1}{3}, \frac{2}{3}, \frac{2}{3}; \frac{2}{3}, \frac{1}{3}, \frac{1}{3}) + 0, 0, z$. The Zn atoms have values of $z = 0, \frac{1}{6}, \frac{7}{12}, \frac{3}{4}$ and the S atoms have values of $z(S) = z(Zn) + \frac{1}{16}$. A trial structure of Cu_2ZnGeS_4 was derived from that of $12R$ ZnS by ordering the metal ions in such a manner that each S atom is coordinated to two Cu, one Ge and one Zn atom in a similar fashion to the ordering in the tetragonal stannite structure. The trial structure was in broad accord with the observed convergent-beam diffraction and lattice-image data.

The structure, a projection of which along the [001] direction is shown in Fig. 5(a), has a triply primitive orthogonal set of axes with ideal axial ratios $b/c = \sqrt{3}/2$ and $a/b = 4\sqrt{2}$. The atomic coordinates of the unit cell are $(0, 0, 0)$ $(\frac{1}{3}, \frac{1}{3}, 0)$ $(\frac{2}{3}, \frac{2}{3}, 0) + (x, y, z)$ with the atom coordinates of different atoms as follows: Zn $\frac{1}{96}, \frac{1}{12}, \frac{1}{4}; \frac{17}{96}, \frac{1}{12}, \frac{1}{4}; \frac{41}{96}, \frac{1}{12}, \frac{3}{4}; \frac{57}{96}, \frac{1}{12}, \frac{3}{4}$; Ge $\frac{1}{96}, \frac{1}{12}, \frac{3}{4}; \frac{17}{96}, \frac{1}{12}, \frac{3}{4}; \frac{41}{96}, \frac{1}{12}, \frac{1}{4}; \frac{57}{96}, \frac{1}{12}, \frac{1}{4}$; Cu $\frac{1}{96}, \frac{7}{12}, 0; \frac{17}{96}, \frac{7}{12}, 0; \frac{41}{96}, \frac{7}{12}, 0; \frac{57}{96}, \frac{7}{12}, 0; \frac{1}{96}, \frac{7}{12}, 0{\cdot}5; \frac{17}{96}, \frac{7}{12}, 0{\cdot}5; \frac{41}{96}, \frac{7}{12}, 0{\cdot}5; \frac{57}{96}, \frac{7}{12}, 0{\cdot}5$.

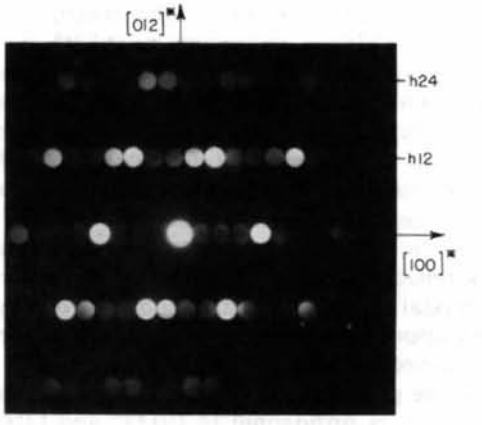

Fig. 9. CBED pattern of the pseudo-rhombohedral (*hhcc*) form of Cu_2ZnGeS_4 ($a = 36{\cdot}6$, $b = 6{\cdot}55$, $c = 7{\cdot}52$ Å) viewed down [0$\bar{3}$2].

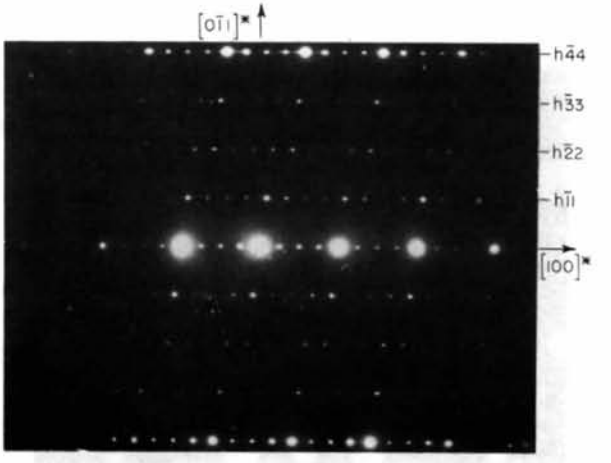

Fig. 10. Selected-area diffraction pattern of the *hhcc* form of Cu_2ZnGeS_4 viewed down [011]. Note the strong sublattice reflections in $h\bar{k}k$ for $h = 4n$.

The S-atom coordinates are given by $(\frac{1}{16}, 0, 0)+$ the metal-atom coordinates.

For the [100] projection of this trial structure allowed $0kl$ reflections have $l=2n$ in addition to the general condition $h+k=3n$. Of these allowed reflections, strong sublattice reflections are given by $l=4n$ for $k=6n$ and $l=4n+2$ for $k=6n+3$. This is in general agreement with the CBED pattern of Fig. 11. For the [001] projection the allowed reflections are given by the condition $h+k=3n$. Of the allowed reflections, strong sublattice reflections arise for the condition $k=2n$ and in particular for $h00$ there is the additional condition $h=12n$. These are in general agreement with the CBED pattern of Fig. 8 and the selected-area pattern of Fig. 12.

Because of the pseudo-rhombohedral geometry of the unit-cell dimensions, the reciprocal axes [012]*, [100]*, and [$0\bar{3}2$]* are very close to orthogonal and collinear with [023], [100] and [$0\bar{2}1$] which correspond to an alternate orthogonal unit cell of dimensions $a'=26{\cdot}6$, $b'=15{\cdot}1$, and $c'=36{\cdot}6$ Å.

Indeed for the projection of the structure down the [$0\bar{2}1$] axis which is orthogonal to [012]* and [100]* a CBED pattern is obtained (Fig. 9) that bears a close resemblance to the [001] projection. The intensities of $hk2k$ reflections are indistinguishable from $\bar{h}2k0$ reflections and the major difference in the diffraction patterns obtained from [001] and [$0\bar{2}1$] is the appearance of weak rows of reflections on the [001] pattern for $k=2n+1$. There are no corresponding rows of weak reflections on the [$0\bar{2}1$] zone axis pattern. The two crystal orientations can of course be distinguished by the upper Laue zones as the repeat distances along the two projection axes are different.

For the projection of the structure down the [011] axis which is orthogonal to [$0\bar{1}1$]* and [100]* (see Fig. 10) intense spots are observed in layer lines $h\bar{k}k$ for $k=4n$.

Lattice images of Cu_2ZnGeS_4 viewed down [001] or [$0\bar{2}1$] are shown in Figs. 13, 14, 15 and 16.

For the images of Fig. 13, the imaging conditions are such that the *hhcc* stacking sequence can be read off directly. Small differences in illumination and defect of focus lead to subtle effects which will be the subject of a separate paper devoted to image calculations in tetrahedral compounds.

In Fig. 14 the superlattice periodicity is apparent but not the stacking sequence, illustrating that there is a limited range of imaging conditions for which intuitive interpretation is valid. This is particularly true for noncentrosymmetric structures where a Niehr's reduction does not have general application.

In Fig. 15 the *hhcc* stacking sequence is interrupted by a quadruple stacking fault, namely four extra slabs of cubic stacking as indicated.

Finally Fig. 16 is a lattice image of *hhcc* stacking in the pseudo-rhombohedral Cu_2ZnGeS_4 with a surface layer of tetragonal material that is in either [021] or [110] orientation.

Refinement of the structure of pseudo-rhombohedral Cu_2ZnGeS_4

The trial structure above is in general accord with the observed lattice images and CBED. However, it is of interest to determine whether an improvement in the accord between calculated and observed lattice images and CBED patterns can be achieved by refinement of the structure. The trial structure has equal bond lengths for Cu–S, Zn–S and Ge–S. By analogy with the structure of the tetrahedral stannite structure we displace each of the sixteen S atoms in the asymmetric unit from the ideal position of the trial structure. The minimum reduction in the local symmetry of a S atom is obtained if the S atom is displaced in the Ge–S–Zn plane so that the S atom

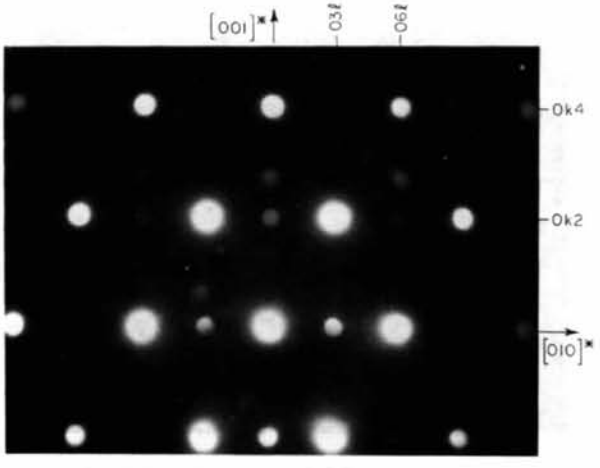

Fig. 11. CBED pattern of the *hhcc* form of Cu_2ZnGeS_4 viewed down [100] showing hexagonal geometry in this projection.

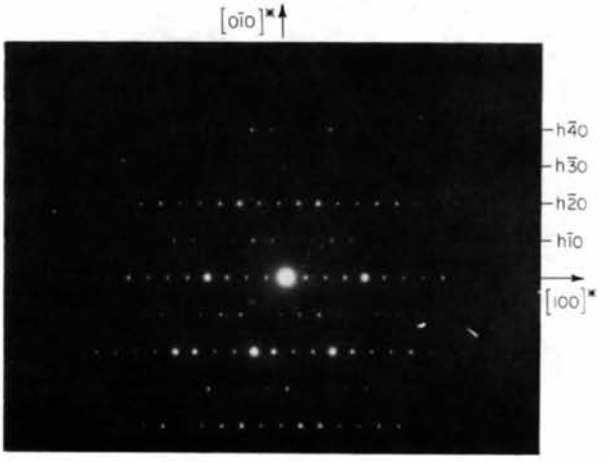

Fig. 12. Selected-area diffraction pattern of the *hhcc* form of Cu_2ZnGeS_4 viewed down [001].

remains equidistant from its two nearest-neighbour Cu atoms. The direction of displacement is such as to be in accord with Cu–S, Zn–S and Ge–S bond lengths (Pauling & Huggins, 1934). For S atoms 1 to 8 the change in position parameter is $(0{\cdot}00106a \pm 0{\cdot}00848b) \pm (0{\cdot}0009a \pm 0{\cdot}0036b)$ and for S atoms 9 to 16 the change in position parameter is $(0{\cdot}00106a \pm 0{\cdot}00848b) \pm (0{\cdot}0054c)$. The positional coordinates for the trial and refined structures are listed in Table 2. The bond lengths of the refined structure are 2·356, 2·311 and 2·243 Å for Cu–S, Zn–S and Ge–S respectively in accord with tetrahedral bond radii (Pauling & Huggins, 1934) and the bond angles at each of the sixteen S atoms in the asymmetric unit are 112·25, 108·24, 110·16 and 106·75° for Zn–S–Ge, Zn–S–Cu, Ge–S–Cu and Cu–S–Cu respectively.

The better agreement of calculated structure factors with the observed CBED pattern is illustrated by comparison of calculated structure factors for $hk0$, $h\bar{k}k$, and $0kl$ (Tables 3, 4) and dynamic intensities for $hk0$ (Table 6) for the ideal and refined structures with observed CBED patterns. In the $hk0$ zone both the ideal and the refined structure factors are zero for $h00$ reflections with $h \neq 12n$, in agreement with the bands observed in the CBED patterns. For the $h30$ reflections, however, the ideal structure gives zero intensity for $h \neq 12n$, whereas for the refined structure the $h30$ reflections are calculated to be all non-zero. Further, the $h\bar{3}3$ reflections for the ideal structure are absent for $k \neq 12n+6$, but are all non-zero for the refined structure. The selected-area pattern of Fig. 10 shows this row of reflections to be all present.

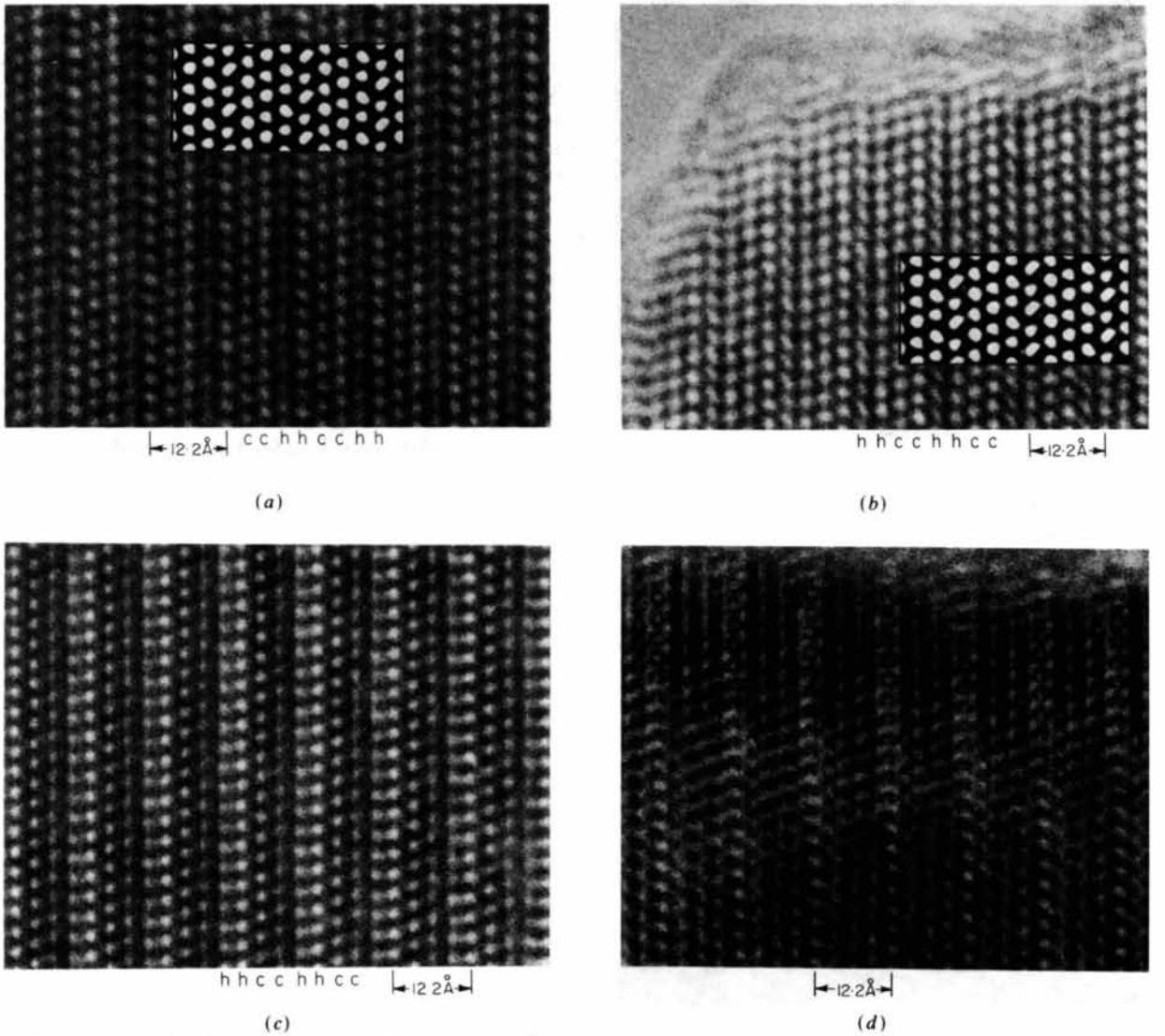

Fig. 13. (*a*)-(*d*) Lattice images of *hhcc* Cu_2ZnGeS_4 viewed down the *c* axis. The stacking sequence is easily recognized in each case. Images calculated by multislice with a defect of focus −600 Å and thickness of 180 Å are inserted in (*a*) and (*b*).

Table 2. *Atomic coordinates of* S *atoms in ideal and refined hhcc* Cu_2ZnGeS_4

	Ideal structure			Refined structure		
	x	*y*	*z*	*x*	*y*	*z*
S(1)	0·07292	0·08333	0·25000	0·07276	0·07125	0·25000
S(2)	0·23958	0·08333	0·25000	0·23942	0·07125	0·25000
S(3)	0·15625	0·75000	0·75000	0·15609	0·76208	0·75000
S(4)	0·32292	0·75000	0·75000	0·32276	0·73792	0·75000
S(5)	0·07292	0·08333	0·75000	0·07096	0·07845	0·75000
S(6)	0·23958	0·08333	0·75000	0·23762	0·07845	0·75000
S(7)	0·15625	0·75000	0·25000	0·15429	0·75488	0·25000
S(8)	0·32292	0·75000	0·25000	0·32096	0·74512	0·25000
S(9)	0·07292	0·58333	0·00000	0·07398	0·59181	0·00540
S(10)	0·23958	0·58333	0·00000	0·24064	0·59181	0·00540
S(11)	0·15625	0·25000	0·00000	0·15731	0·24152	0·99460
S(12)	0·32292	0·25000	0·00000	0·32398	0·25848	0·99460
S(13)	0·07292	0·58333	0·50000	0·07398	0·59181	0·49460
S(14)	0·23958	0·58333	0·50000	0·24064	0·59181	0·49460
S(15)	0·15625	0·25000	0·50000	0·15731	0·24152	0·50540
S(16)	0·32292	0·25000	0·50000	0·32398	0·25848	0·50540

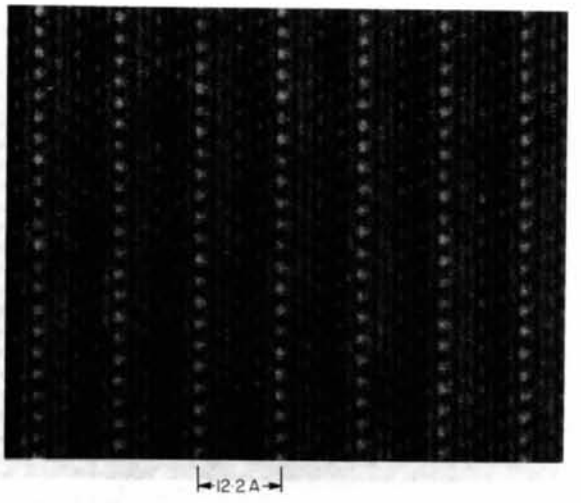

Fig. 14. Lattice image of *hhcc* Cu_2ZnGeS_4 viewed down the *c* axis. The superlattice periodicity is obvious but the stacking sequence is not clear from this micrograph.

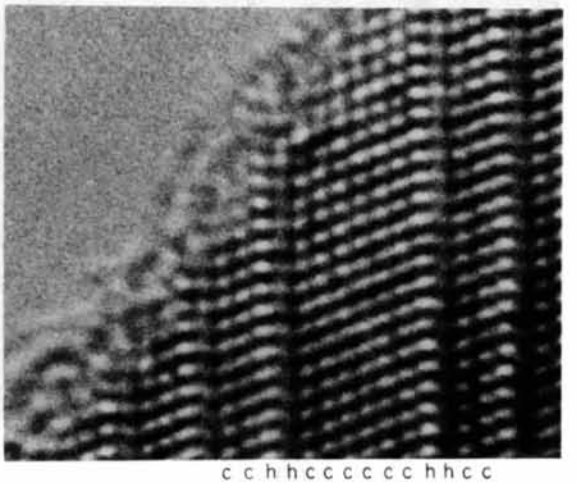

Fig. 15. Lattice image of *hhcc* Cu_2ZnGeS_4 viewed down the *c* axis showing the stacking fault with sequence *hhcchhcccccchhcc*.

In Table 5 are compared the calculated structure factors of $hk2k$ and $\bar{h}2k0$ beams for the refined structure of *hhcc* Cu_2ZnGeS_4. While the amplitude of these strong sublattice beams hardly differs in agreement with the CBED patterns of the two zones (Figs. 8 and 9), the phases are related with the approximate symmetries of the sublattice.

Thickness fringes for the central beam and the main beams that determine the lattice images of *hhcc* Cu_2ZnGeS_4 viewed down [001] are shown in Fig. 17. The fringes graphically emphasize the breakdown of Friedel's law in this particular projection of the non-centrosymmetric structure.

A series of images was calculated for the refined structure of Cu_2ZnGeS_4 at representative defects of focus and thickness (Fig. 18) using D. Lynch's version of the multislice programs and incorporating instrumental parameters determined by optical interferometry.

Only positional parameters were refined, neutral atomic scattering factors being used throughout. While in the final analysis such simplifications are invalid the current aim was to determine the structure in the sense of locating the positions of the nucleii to within 0·1 Å.

Discussion of the structure

The main features that characterize the CBED of the *hhcc* form of Cu_2ZnGeS_4 may be summarized as follows. The principal projections of the structure consist of a set of intense sublattice peaks and a set of considerably weaker superlattice peaks. In the $00l$ projection the strong beams are the $hk0$ with k even while the $hk0$ with k odd are all weak. The $h00$ reflections are a special case in that these are all

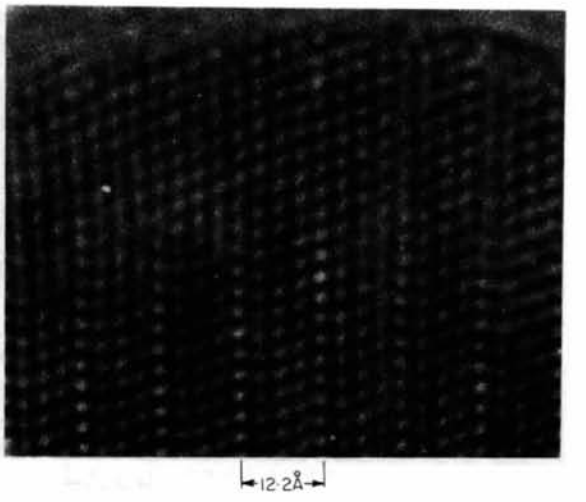

Fig. 16. Lattice image of pseudo-rhombohedral (*hhcc*) Cu_2ZnGeS_4 viewed down the *c* axis with a surface layer martensitically transformed to tetragonal (*ccc*) Cu_2ZnGeS_4.

Table 3. *Calculated hk0 and hk̄k structure factors (in volts) for ideal and refined hhcc* Cu_2ZnGeS_4

	Ideal		Refined	
h k l	V_R	V_I	V_R	V_I
0 0 0	13·820	0·000	13·820	0·000
12 0 0	6·248	0·432	6·235	0·445
$\bar{7}$ 1 0	0·361	−0·072	0·468	−0·118
$\bar{4}$ 1 0	−0·093	0·093	−0·170	0·170
$\bar{1}$ 1 0	0·025	−0·125	0·051	−0·241
2 1 0	0·092	0·224	0·186	0·427
5 1 0	0·348	0·232	0·591	0·414
$\bar{8}$ 1 0	−0·102	0	−0·103	0
$\overline{14}$ 2 0	2·392	−0·105	2·392	−0·116
$\overline{11}$ 2 0	−0·863	0·114	−0·864	0·126
$\bar{8}$ 2 0	0	−0·151	0	−0·163
$\bar{5}$ 2 0	4·023	0·423	4·017	0·440
$\bar{2}$ 2 0	3·659	0·102	3·649	0·104
1 2 0	−2·027	0·027	−2·021	0·027
4 2 0	1·566	−0·108	1·563	−0·111
7 2 0	−1·331	0·496	−1·330	0·528
10 2 0	1·201	0·243	1·202	0·267
13 2 0	−1·173	−0·078	−1·173	−0·086
16 2 0	1·345	0	1·342	0
19 2 0	−3·172	0·306	−3·145	0·333
12 3 0	−0·055	0·055	−0·186	−0·189
9 3 0	0	0	0·163	−0·106
6 3 0	0	0	−0·197	0·080
3 3 0	0	0	0·222	−0·043
0 3 0	0	0·152	0·231	0·149
$\bar{3}$ 3 0	0	0	0·222	0·043
$\bar{6}$ 3 0	0	0	−0·197	−0·080
$\bar{9}$ 3 0	0	0	0·163	0·106
$\overline{12}$ 3 0	0·055	0·055	0·061	0·050
$\overline{11}$ $\bar{1}$ 1	−0·105	−0·070	−0·014	−0·046
$\bar{8}$ $\bar{1}$ 1	−0·086	0	−0·083	0·019
$\bar{5}$ $\bar{1}$ 1	0·045	−0·030	0·060	−0·049
$\bar{2}$ $\bar{1}$ 1	−0·026	0·062	−0·038	0·093
1 $\bar{1}$ 1	−0·045	−0·226	−0·068	−0·334
4 $\bar{1}$ 1	0·078	−0·078	−0·109	−0·120
7 $\bar{1}$ 1	0·047	0·009	0·053	0·022
10 $\bar{1}$ 1	−0·039	0·016	−0·019	0·008
$\overline{10}$ $\bar{2}$ 2	−0·021	0·051	0·219	0·104
$\bar{7}$ $\bar{2}$ 2	0·027	0·134	0·312	0·075
$\bar{4}$ $\bar{2}$ 2	−0·034	−0·034	0·011	0·011
$\bar{1}$ $\bar{2}$ 2	0·046	0·009	−0·085	−0·007
2 $\bar{2}$ 2	−0·082	0·034	0·132	−0·022
5 $\bar{2}$ 2	−0·086	0·128	−0·089	−0·012
8 $\bar{2}$ 2	0·0	−0·038	0·115	−0·037
11 $\bar{2}$ 2	0·014	0·022	−0·104	0·058
$\bar{9}$ $\bar{3}$ 3	0·0	0·0	−0·011	0·018
$\bar{6}$ $\bar{3}$ 3	0·031	−0·013	0·112	0·008
$\bar{3}$ $\bar{3}$ 3	0·0	0·0	−0·004	0·024
0 $\bar{3}$ 3	0·0	0·0	0·0	−0·024
3 $\bar{3}$ 3	0·0	0·0	0·004	0·023
6 $\bar{3}$ 3	0·031	0·013	0·128	0·035
9 $\bar{3}$ 3	0·0	0·0	0·011	0·018
$\overline{11}$ $\bar{4}$ 4	0·306	−0·107	0·300	−0·109
$\bar{8}$ $\bar{4}$ 4	0·0	0·147	0·0	0·153
$\bar{5}$ $\bar{4}$ 4	−1·260	−0·417	−1·242	−0·441
$\bar{2}$ $\bar{4}$ 4	−1·109	−0·100	−1·096	−0·107
1 $\bar{4}$ 4	0·611	−0·026	0·604	−0·028
4 $\bar{4}$ 4	−0·484	0·106	−0·477	0·113
7 $\bar{4}$ 4	0·432	−0·487	0·424	−0·508
10 $\bar{4}$ 4	−0·416	−0·232	−0·408	−0·237

Table 4. *Calculated structure factors (in volts) for 0kl beams of ideal and refined hhcc* Cu_2ZnGeS_4

	Ideal		Refined	
h k l	V_R	V_I	V_R	V_I
0 3 0	0	0·1524	0·2305	0·1491
0 6 0	−2·1649	0	−2·1201	−0·0006
0 9 0	0·0	0·0090	−0·0589	−0·0066
0 3 1	0	0	0	0·0498
0 6 1	0	0	−0·0234	0
0 9 1	0	0	0	−0·0124
0 0 2	−0·4072	0	−0·4126	0
0 3 2	0·0	−5·3993	0	−5·3635
0 6 2	0·0121	0	0·0097	−0·1155
0 9 2	0·0	0·6924	0·0005	0·6626
0 3 3	0	0	0	−0·0243
0 6 3	0	0	0·0264	0
0 9 3	0	0	0	0·0074
0 0 4	5·3991	0	5·3881	0
0 3 4	0·0	0·0317	0·1161	0·0367
0 6 4	−1·5588	0	−1·5252	0
0 9 4	0·0	−0·0080	−0·0459	−0·0070
0 3 5	0	0	0	0·0258
0 6 5	0	0	−0·0089	0
0 9 5	0	0	0	−0·0114
0 0 6	−0·0192	0	−0·0309	0
0 3 6	0·0	−2·1648	−0·0006	−2·1452
0 6 6	0·0101	0	0·0122	−0·0596
0 9 6	0·0	0·4334	0	0·4136
0 3 7	0	0	0	−0·0044
0 6 7	0	0	0·0156	0
0 9 7	0	0	0	0·0022
0 0 8	1·5587	0	1·5483	0
0 3 8	0·0	0·0104	0·0348	0·0180
0 6 8	−0·6924	0	−0·6748	0·0005
0 9 8	0·0	−0·0053	−0·0232	−0·0060

Table 5. *Calculated structure factors (in volts) for h 2k 0 and h̄ k 2k of refined hhcc* Cu_2ZnGeS_4

h k l	V_R	V_I	*h k l*	V_R	V_I
$\overline{14}$ 2 0	2·392	−0·116	14 1 2	0·105	−2·377
$\overline{11}$ 2 0	−0·864	0·126	11 1 2	−0·115	0·858
$\bar{8}$ 2 0	0	−0·163	8 1 2	0·153	0
$\bar{5}$ 2 0	4·017	0·440	5 1 2	−0·434	−4·013
$\bar{2}$ 2 0	3·649	0·104	2 1 2	−0·106	−3·653
1 2 0	−2·021	0·027	$\bar{1}$ 1 2	−0·028	2·024
4 2 0	1·563	−0·111	$\bar{4}$ 1 2	0·111	1·563
7 2 0	−1·330	0·528	$\bar{7}$ 1 2	−0·505	1·326
10 2 0	1·202	0·267	$\overline{10}$ 1 2	−0·245	−1·195
13 2 0	−1·173	−0·086	$\overline{13}$ 1 2	0·078	1·165
$\overline{10}$ 4 0	−0·627	0·270	10 2 4	0·639	0·278
$\bar{7}$ 4 0	0·665	0·571	7 2 4	−0·674	0·563
$\bar{4}$ 4 0	−0·756	−0·126	4 2 4	0·763	−0·120
$\bar{1}$ 4 0	0·962	0·032	1 2 4	−0·968	0·029
2 4 0	−1·743	0·120	$\bar{2}$ 2 4	1·754	0·111
5 4 0	−1·960	0·493	$\bar{5}$ 2 4	1·980	0·472
8 4 0	0	−0·172	$\bar{8}$ 2 4	0	−0·172
11 4 0	0·458	0·125	$\overline{11}$ 2 4	−0·467	0·129
14 4 0	−1·340	0·108	$\overline{14}$ 2 4	1·368	−0·114

forbidden or extremely weak, for h not equal to $12n$, if the incident beam is at exactly normal incidence. As a result there is a strong decoupling of the sublattice from the superlattice and indeed there is decoupling of various parts of the sublattice from each other, an effect similar to the surface superlattice reflections discussed by Spence (1983).

In the present case certain pseudo three-beam interactions can be discerned both experimentally and by multislice calculation of CBED patterns. This particular matter will be the subject of a separate more technical discussion in a later communication.

There are very strong dynamic interactions of the sublattice beams that are evidenced experimentally in observed CBED patterns and in comparison of calculated structure factors (Tables 3, 4, 5) with multibeam calculated intensities (Table 6) for Friedel pairs. Because of the strong decoupling of the strong sublattice and the weaker superlattice reflections, the dynamic interactions for weaker reflections are much less at a given thickness of crystal and a comparison of calculated structure factors for these weaker superlattice reflections with observed intensities may be used for initial refinement of the ideal structure.

The sublattice contains information on the *hhcc* stacking as well as most of the information about the projected atom peaks. For the reasons given, this is heavily decoupled from the remaining superlattice which refers to non-ideal positions of the S atoms. Comparison of calculated structure factors for the ideal and refined structure identifies those weak superlattice reflections that are most affected by small changes in the S-atom positions. A first-order refinement of the structure can then be made using comparison of the structure amplitudes of the weak to very weak reflections with observed CBED intensities. Indeed this structure is an ideal one for a comprehensive refinement using, for example, rocking-beam curves on the forbidden superlattice 100 and 200 reflections to give precise measurement of potential in the Cu–S, Zn–S and Ge–S bonds. Such a refinement is planned as the subject of a subsequent publication.

Although the sequences of hexagonal and cubic packed layers have been identified for a large number of polytypes of SiC, ZnS and related compounds (Parthé, 1972), there are few reported observations of adjacent hexagonally stacked layers other than the $2H$ polytypes that consist of complete hexagonal stacking. For ZnS one mineral sample was found to contain adjacent hexagonally stacked layers in the form of the polytypes $9R$ (*hhc*), $12R$ (*hhcc*) and $21R$ (*hhhchccc*) (Haussuehl & Mueller, 1963). For hexastannite (Cu_2FeSnS_4) (Ramdohr, 1944; Moh & Otteman, 1962) the X-ray powder pattern can be indexed for a hexagonal lattice with $a = 3{\cdot}84$ and $c = 12{\cdot}6$ Å. The stacking sequence might be either *hchc* indicating a pseudo $4H$ structure or *hhcc* in accord with a pseudo $12R$ structure.

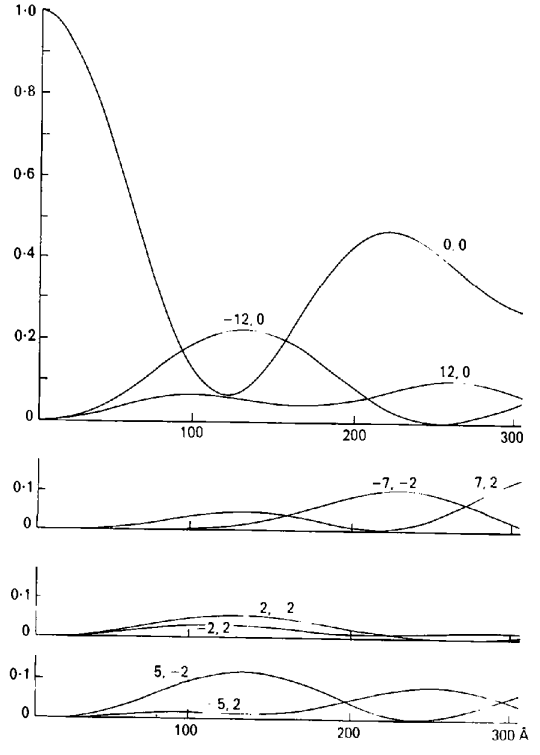

Fig. 17. Multislice calculation of thickness fringes for *hhcc* Cu_2ZnGeS_4 for the central beam and the 12.00, $\bar{1}2.00$, 720, $\bar{7}20$, $2\bar{2}0$, $\bar{2}20$, $5\bar{2}20$ and $\bar{5}20$ beams.

Table 6. *Calculated normalized intensities of hk*0 *beams for* 189 Å *thick crystal of hhcc* Cu_2ZnGeS_4

h k l	Ideal	Refined	*h k l*	Ideal	Refined
12 0 0	0·0465	0·0470	$\bar{1}2$ 0 0	0·1132	0·1098
$\bar{2}2$ 1 0	0·0001	0·0003	22 $\bar{1}$ 0	0·0001	0·0001
$\bar{1}9$ 1 0	0·0002	0·0002	19 $\bar{1}$ 0	0·0004	0·0004
$\bar{1}6$ 1 0	0·0001	0·0001	16 $\bar{1}$ 0	0·0000	0·0001
$\bar{1}3$ 1 0	0·0001	0·0002	13 $\bar{1}$ 0	0·0001	0·0003
$\bar{1}0$ 1 0	0·0004	0·0012	10 $\bar{1}$ 0	0·0004	0·0017
$\bar{7}$ 1 0	0·0032	0·0066	7 $\bar{1}$ 0	0·0026	0·0047
$\bar{4}$ 1 0	0·0006	0·0008	4 $\bar{1}$ 0	0·0003	0·0002
$\bar{1}$ 1 0	0·0005	0·0005	1 $\bar{1}$ 0	0·0004	0·0003
2 1 0	0·0013	0·0007	$\bar{2}$ $\bar{1}$ 0	0·0020	0·0023
5 1 0	0·0033	0·0023	$\bar{5}$ $\bar{1}$ 0	0·0055	0·0084
8 1 0	0·0002	0·0005	$\bar{8}$ $\bar{1}$ 0	0·0002	0·0005
11 1 0	0·0001	0·0004	$\bar{1}1$ $\bar{1}$ 0	0·0001	0·0003
14 1 0	0·0001	0·0007	$\bar{1}4$ $\bar{1}$ 0	0·0003	0·0006
17 1 0	0·0004	0·0010	$\bar{1}7$ $\bar{1}$ 0	0·0005	0·0004
20 1 0	0·0000	0·0000	$\bar{2}0$ $\bar{1}$ 0	0·0000	0·0000
$\bar{2}0$ 2 0	0·0005	0·0005	20 $\bar{2}$ 0	0·0001	0·0001
$\bar{1}7$ 2 0	0·0034	0·0036	17 $\bar{2}$ 0	0·0035	0·0035
$\bar{1}4$ 2 0	0·0070	0·0069	14 $\bar{2}$ 0	0·0034	0·0034
$\bar{1}1$ 2 0	0·0057	0·0056	11 $\bar{2}$ 0	0·0006	0·0005
$\bar{8}$ 2 0	0·0077	0·0076	8 $\bar{2}$ 0	0·0003	0·0003
$\bar{5}$ 2 0	0·0391	0·0399	5 $\bar{2}$ 0	0·0554	0·0537
$\bar{2}$ 2 0	0·0141	0·0136	2 $\bar{2}$ 0	0·0296	0·0285
1 2 0	0·0078	0·0075	$\bar{1}$ $\bar{2}$ 0	0·0053	0·0051
4 2 0	0·0072	0·0070	$\bar{4}$ $\bar{2}$ 0	0·0029	0·0030
7 2 0	0·0135	0·0130	$\bar{7}$ $\bar{2}$ 0	0·0715	0·0713
10 2 0	0·0008	0·0007	$\bar{1}0$ $\bar{2}$ 0	0·0247	0·0241
13 2 0	0·0010	0·0010	$\bar{1}3$ $\bar{2}$ 0	0·0031	0·0030
16 2 0	0·0006	0·0006	$\bar{1}6$ $\bar{2}$ 0	0·0006	0·0006
19 2 0	0·0013	0·0010	$\bar{1}9$ $\bar{2}$ 0	0·0041	0·0041
$\bar{1}8$ 3 0	0·00001	0·00009	18 $\bar{3}$ 0	0·00001	0·00000
$\bar{1}5$ 3 0	0·00002	0·00016	15 $\bar{3}$ 0	0·00001	0·00000
$\bar{1}2$ 3 0	0·00062	0·00065	12 $\bar{3}$ 0	0·00022	0·00080
$\bar{9}$ 3 0	0·00002	0·00036	9 $\bar{3}$ 0	0·00001	0·00002
$\bar{6}$ 3 0	0·00002	0·00040	6 $\bar{3}$ 0	0·00001	0·00005
$\bar{3}$ 3 0	0·00001	0·00034	3 $\bar{3}$ 0	0·00000	0·00013
0 3 0	0·00066	0·00110	0 $\bar{3}$ 0	0·00090	0·00083
3 3 0	0·00000	0·00013	$\bar{3}$ $\bar{3}$ 0	0·00001	0·00035
6 3 0	0·00000	0·00006	$\bar{6}$ $\bar{3}$ 0	0·00002	0·00039
9 3 0	0·00000	0·00002	0 $\bar{3}$ 0	0·00002	0·00035
12 3 0	0·00065	0·00102	$\bar{1}2$ $\bar{3}$ 0	0·00092	0·00275
15 3 0	0·00001	0·00000	$\bar{1}5$ $\bar{3}$ 0	0·00002	0·00017
18 3 0	0·00001	0·00000	$\bar{1}8$ $\bar{3}$ 0	0·00001	0·00009
$\bar{1}9$ 4 0	0·0008	0·0008	19 $\bar{4}$ 0	0·0016	0·0015
$\bar{1}6$ 4 0	0·0001	0·0000	16 $\bar{4}$ 0	0·0001	0·0001
$\bar{1}3$ 4 0	0·0001	0·0001	13 $\bar{4}$ 0	0·0002	0·0002
$\bar{1}0$ 4 0	0·0004	0·0003	10 $\bar{4}$ 0	0·0027	0·0028
$\bar{7}$ 4 0	0·0023	0·0021	7 $\bar{4}$ 0	0·0110	0·0105
$\bar{4}$ 4 0	0·0005	0·0005	4 $\bar{4}$ 0	0·0001	0·0001
$\bar{1}$ 4 0	0·0005	0·0005	1 $\bar{4}$ 0	0·0002	0·0002
2 4 0	0·0002	0·0002	$\bar{2}$ $\bar{4}$ 0	0·0019	0·0019
5 4 0	0·0043	0·0038	$\bar{5}$ $\bar{4}$ 0	0·0042	0·0040
8 4 0	0·0011	0·0011	$\bar{8}$ $\bar{4}$ 0	0·0002	0·0001
11 4 0	0·0005	0·0005	$\bar{1}1$ $\bar{4}$ 0	0·0001	0·0001
14 4 0	0·0003	0·0004	$\bar{1}4$ $\bar{4}$ 0	0·0002	0·0002
17 4 0	0·0015	0·0013	$\bar{1}7$ $\bar{4}$ 0	0·0006	0·0005
20 4 0	0·0001	0·0001	$\bar{2}0$ $\bar{4}$ 0	0·0001	0·0001
$\bar{1}8$ 6 0	0·00003	0·00003	18 $\bar{6}$ 0	0·00003	0·00003
$\bar{1}5$ 6 0	0·00004	0·00003	15 $\bar{6}$ 0	0·00003	0·00003
$\bar{1}2$ 6 0	0·00066	0·00056	12 $\bar{6}$ 0	0·00028	0·00027
$\bar{9}$ 6 0	0·00002	0·00002	9 $\bar{6}$ 0	0·00001	0·00001
$\bar{6}$ 6 0	0·00002	0·00002	6 $\bar{6}$ 0	0·00001	0·00001
$\bar{3}$ 6 0	0·00001	0·00002	3 $\bar{6}$ 0	0·00001	0·00001
0 6 0	0·00021	0·00016	0 $\bar{6}$ 0	0·00023	0·00018
3 6 0	0·00001	0·00001	$\bar{3}$ $\bar{6}$ 0	0·00001	0·00001
6 6 0	0·00001	0·00001	$\bar{6}$ $\bar{6}$ 0	0·00002	0·00002
9 6 0	0·00001	0·00001	$\bar{9}$ $\bar{6}$ 0	0·00002	0·00002
12 6 0	0·00013	0·00012	$\bar{1}2$ $\bar{6}$ 0	0·00130	0·00114
15 6 0	0·00003	0·00003	$\bar{1}5$ $\bar{6}$ 0	0·00004	0·00003
18 6 0	0·00003	0·00003	$\bar{1}8$ $\bar{6}$ 0	0·00003	0·00003

Conclusion

The structure of a pseudo-rhombohedral polymorph of Cu_2ZnGeS_4 has been determined by a combination of lattice imaging and convergent-beam and selected-area electron diffraction.

The unusual stacking sequence *hhcc* of this polymorph was determined by direct interpretation of lattice images obtained with 200 kV electrons. The intensity distribution of the sublattice reflections of electron diffraction patterns of crystals in several orientations confirmed the outline structure. The ordering of cations was determined, and initial refinement of S-atom positions was achieved, from details of the superlattice, such as dark bands on some CBED discs and the absence or presence of other reflections.

Various dynamical effects, most obviously the breakdown of Friedel's law, were found to be decisive aids at various stages in the determination of the structure; for instance the unequivocal assignment of the space groups.

A second polymorph of $Cu_2ZnGeS4$ was shown by CBED to have the same ordering in cubic stacking and thus to be tetragonal and isostructural with stannite Cu_2FeSnS_4.

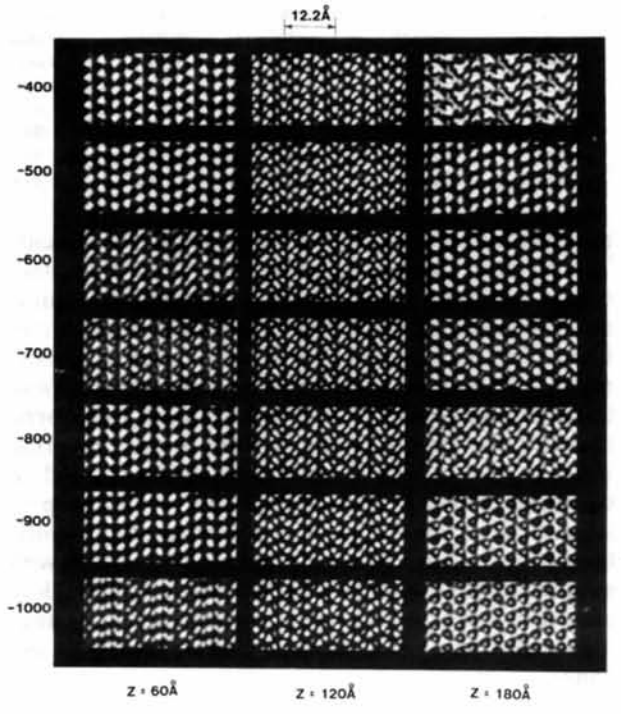

Fig. 18. Multislice calculations using C_s of 0·94 mm of the refined *hhcc* Cu_2ZnGeS_4 structure viewed down the *c* axis with 200 kV electrons. Calculations are presented for seven defects of focus (Å) as indicated at the left of the diagram for each of three thicknesses z=60, 120 and 180 Å as indicated at the bottom of the diagram.

References

AMELINCKX, S. (1979). *Dislocations in Solids.* Vol. 2, ch. 6, edited by F. R. N. NABARRO. Amsterdam: North-Holland.

BROCKWAY, L. O. (1934). *Z. Kristallogr.* **89**, 434–441.

HAUSSUEHL, S. & MUELLER, G. (1963). *Beitr. Mineral. Petrogr.* **9**, 28–33. (*Chem. Abstr.* **59**: 4905d.)

MOH, G. H. & OTTEMAN, J. (1962). *Neues Jahrb. Mineral Abh.* **99**, 1–28

MOODIE, A. F. & WHITFIELD, H. J. (1983). *Acta Cryst.* A**30**, 946–947.

MOODIE, A. F. & WHITFIELD, H. J. (1984). *Ultramicroscopy*, **13**, 265–278.

OLSEN, A. & SPENCE, J. C. H. (1981). *Philos. Mag.* **43**, 945–965.

PARTHÉ, E. (1972). *Cristallochimie des Structures Tetraédriques.* New York, London: Gordon and Breach.

PAULING, L. & HUGGINS, M. L. (1934). *Z. Kristallogr.* **87**, 205–238.

RAMDOHR, P. (1944). *Abh. Preuss, Akad. Wiss.* **4**, No. 4. (*Chem. Abstr.* **40**: 6023°.)

SAYRE, D. (1951). *Acta Cryst.* **4**, 60–65.

SPENCE, J. C. H. (1983). *Ultramicroscopy*, **11**, 117–124.

Acta Cryst. (1986). B**42**, 247–253

Electron Charge Density and Electron Momentum Distribution in Magnesium Oxide

BY M. CAUSA', R. DOVESI, C. PISANI AND C. ROETTI

Institute of Theoretical Chemistry, University of Turin, Via P. Giuria 5, *I*-10125 *Torino, Italy*

(*Received* 23 *July* 1985; *accepted* 23 *December* 1985)

Abstract

The electronic structure of magnesium oxide is presented and discussed, as resulting from a LCAO crystalline-orbital Hartree–Fock extended-basis-set computation. Mulliken populations, charge density maps, structure factors, electron momentum distribution and Compton profiles are provided. They are compared with the results of simple theoretical models, and with available experimental data. The present study confirms the fully ionic character of MgO; it also shows that there is a certain anisotropy of the oxygen ion in the crystalline environment, and that the magnesium ion is slightly expanded with respect

0108-7681/86/030247-07$01.50